Journal of Physics D: Applied Physics

PAPER • OPEN ACCESS

Effect of precursor pH on AuNP/MWCNT nanocomposites synthesized by plasma-induced non-equilibrium electrochemistry

To cite this article: Daye Sun *et al* 2020 *J. Phys. D: Appl. Phys.* **53** 425207

OPEN ACCESS
IOP Publishing
Journal of Physics D: Applied Physics
J. Phys. D: Appl. Phys. **53** (2020) 425207 (9pp)
https://doi.org/10.1088/1361-6463/ab9ee7

Effect of precursor pH on AuNP/MWCNT nanocomposites synthesized by plasma-induced non-equilibrium electrochemistry

Daye Sun[1], Chiranjeevi Maddi[2], Cormac Rafferty[3], Miao Tang[4], Mei Chen[4], Brian G Falzon[1], Gianluca Sarri[3], Davide Mariotti[2], Paul Maguire[2] and Dan Sun[1,7]

[1] Advanced Composites Research Group (ACRG), School of Mechanical and Aerospace Engineering, Queen's University, Belfast BT9 5AH, United Kingdom
[2] Nanotechnology and Integrated Bioengineering Centre, Ulster University, Co Antrim BT37 OQB, United Kingdom
[3] School of Mathematics and Physics, Queen's University, Belfast BT7 1NN, United Kingdom
[4] The Wellcome-Wolfson Institute of Experimental Medicine, School of Medicine, Dentistry and Biomedical Sciences, Queen's University, Belfast BT9 7BL, United Kingdom
[5] School of Electronic and Electrical Engineering, University of Leeds, Leeds LS2 9JT, United Kingdom
[6] Leeds Institute of Cancer and Pathology, University of Leeds, Leeds LS2 9JT, United Kingdom

E-mail: d.sun@qub.ac.uk

Received 21 April 2020, revised 18 June 2020
Accepted for publication 22 June 2020
Published 29 July 2020

Abstract

In recent years, plasma-induced non-equilibrium electrochemistry (PiNE) has been increasingly used for the synthesis of nanomaterials. In this study, we investigated the effect of solution pH on the formation of AuNP/MWCNT nanocomposites synthesized by PiNE. It is found that resulting nanocomposite morphology can be manipulated by the solution pH with pH 2 giving the most uniformly distributed AuNP along the MWCNT surface during the nanocomposite formation. The detailed mechanisms of AuNP/MWCNT nanocomposites formation under different pH have been discussed. For selected AuNP/MWCNT, we further evaluated the photothermal conversion performance under a blue laser (wavelength 445 nm) and the material biocompatibility using HeLa cells. The promising photothermal capability and biocompatibility of the composite sample point to their potential future applications such as solar thermal conversion and healthcare technology.

Supplementary material for this article is available online

Keywords: plasma-induced non-equilibrium electrochemistry, AuNP/MWCNT nanocomposites, pH, photothermal conversion, biocompatibility

(Some figures may appear in colour only in the online journal)

[7] Author to whom any correspondence must be addressed.

1. Introduction

In recent years, there has been an increasing volume of research in deploying atmospheric pressure plasma for a wide range of applications ranging from healthcare to environmental remediation and material science [1–3]. In the field of material synthesis, atmospheric pressure microplasma (APM)–liquid interaction and PiNE has been successfully deployed for applications such as surface functionalization of nanostructures (e.g. carbon nanomaterials [4] and Si nanocrystals [5]), synthesis of metal nanoparticles (NPs) (e.g. AuNPs [6] and AgNPs [7]) and metal oxides such as Fe_3O_4 [8], CuO [9], and Co_3O_4 [10]. Out of these studies, AuNPs synthesized by APM is of particular interest, due to the unique physical and chemical properties of the nanoparticles [11–13].

Recently, researchers have taken a step further to synthesize AuNP based functional nanocomposites, such as AgNP/polyvinyl alcohol (PVA) for antibacterial action [14], AuNP/PEDOT:PSS for potential fuel cell electro-catalyst [15], and AuNP/graphene oxide (GO) for biosensing applications [16]. Early studies also demonstrated the capability of APM in the synthesis of AuNP/carbon nanotube (CNT) nanocomposites [17, 18]. The combination of plasmonic AuNPs with multiwall carbon nanotube (MWCNT) has led to nanocomposites with strong photothermal conversion capability under near infrared laser (NIR, 852 nm) irradiation. The photothermal conversion efficiency of the as-synthesized nanocomposite was also much higher than that of the individual constituents (i.e. pure AuNPs or MWCNT), due to synergistic effects.

In this work, we further investigated the effect of different solution pH on the resulting structures of the AuNP/CNT nanocomposites synthesized by PiNE and the formation mechanisms under different pH conditions have been discussed. In addition, the photothermal conversion of the AuNP/CNT under a blue laser irradiation (445 nm) has been demonstrated and the cytotoxicity of the composite was also evaluated.

2. Experimental details

2.1. APM set-up description

The direct current (DC) APM set-up used in this work is shown in figure 1. A carbon rod was deployed as anode while the cathode was a hollow stainless-steel capillary (250 μm inner diameter). The anode and cathode were placed vertically ~2 cm apart. The cathode was placed 1 mm above the surface of the aqueous solution, while the anode was immersed in the solution. Helium gas (25 sccm) was supplied through the capillary and the microplasma was ignited at the gas liquid interface at an initial applied DC voltage of ~2 kV. After the microplasma was ignited, the current was adjusted to 5 mA and maintained for 10 min for all sample treatment. It was observed that the voltage gradually dropped over the treatment time and stabilized at 0.9–1 kV for all samples, which indicates an increases of solution conductivity in line with the literature [19]. The temperature of the bulk solution was always below 40 °C throughout the treatment process.

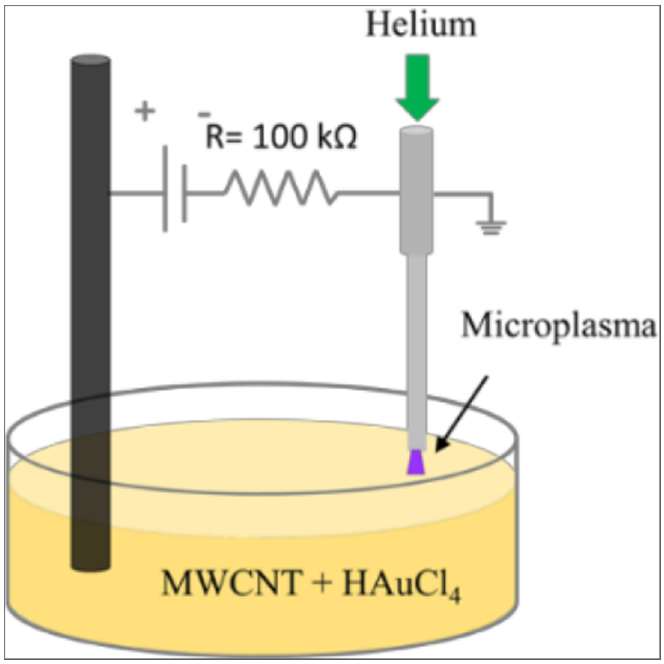

Figure 1. Schematic of the APM set-up deployed in this work.

2.2. Synthesis of AuNP/MWCNT nanocomposites

Hydrogen tetrachloroaurate (III) ($HAuCl_4 \cdot 3H_2O$, >99.9%) was supplied by Sigma Aldrich. Carboxyl group (-COOH) functionalized multi-walled carbon nanotubes (MWCNTs, purity >95 wt%, length 10–30 μm, diameter 20–30 nm) were purchased from Cheap Tubes Inc. 0.1 mg ml^{-1} MWCNTs aqueous mixture (prepared using 18.2 MΩ cm^{-1} deionized water from a Millipore Milli-Q machine) was sonicated for 6 h under 140 W power. The dispersed MWCNTs supernatant was collected and further diluted by distilled water to obtain a 50 ± 3 μg ml^{-1} aqueous solution.

Mixture of $HAuCl_4$/MWCNT with 0.1 mM $HAuCl_4$ were prepared by mixing proper amount $HAuCl_4$ solution (5 mM) and the diluted MWCNTs solution (50 ± 3 μg ml^{-1}); this solution exhibited a pH of 2, very likely due to the presence of $HAuCl_4$ and the de-protonation of the -COOH CNT terminations. Afterwards, sodium hydroxide (NaOH, Sigma Aldrich) was used to adjust the solution pH of 0.1 mM $HAuCl_4$/MWCNT to 7 and 12, respectively. 0.1 mM $HAuCl_4$/MWCNT mixtures with different pH (2, 7, and 12) were settled for 30 min before treated by PiNE under the same processing parameters. All samples mentioned in this work were treated by PiNE at a current of 5 mA for 10 min, the resulting composite samples were named as AuNP/MWCNT-pH2, AuNP/MWCNT-pH7, and AuNP/MWCNT-pH12. Pure 0.1 mM AuNPs (prepared using the same parameters without MWCNTs) synthesized under different pH (pH 2, 7 and 12) were used as reference samples, and they were named as AuNP-pH2, AuNP-pH7, and AuNP-pH12, respectively.

2.3. Characterization

A Cary 60 UV–Vis (Agilent Technologies) spectrophotometer was used to examine the optical properties of all samples. A

Jeol JEM 1400-plus transmission electron microscope (TEM) was used to analyse the morphologies of the AuNP/MWCNT nanocomposites. The size distribution of AuNPs was analysed using an open source ImageJ software using >100 particles from each sample. The diameter was measured for spherical NPs, while for NPs with other morphologies, the longest dimension was measured. X-ray photoelectron spectroscopy (XPS) analysis was performed by using an ESCALAB 250Xi spectrometer microprobe (Thermo Fisher Scientific) with a focused monochromatic AlKα x-ray source ($h\nu = 1486.6$ eV, <900 μm spot size) and the photoelectrons were collected using a 180° double-focusing hemispherical analyzer with a dual detector. The binding energy scale was calibrated with respect to the Au $4f_{7/2}$ peak at 84.00 eV. For all the samples analysed, the survey spectra were recorded with a step size of 1 eV and a pass energy of 150 eV and the narrow scans were recorded with a step size of 0.1 eV and a pass energy of 20 eV. Data analysis and fitting were performed with Avantage software. Deconvoluted C1s peak components were adjusted using asymmetric line shapes using line shapes consisting of a convolution product of a Gaussian function (75%) and Lorentzian function (25%).

2.4. Laser irradiation tests

AuNP/MWCNT-pH2 nanocomposite was selected for photothermal conversion experiment using a blue laser (445 nm wavelength, 1 W, KALE CNC). 2 ml of as-obtained AuNP/MWCNT-pH2 colloid was placed inside a quartz cuvette, the aqueous solution was irradiated by the laser for 15 min. The temperature of the solution was recorded using a thermocouple (RS-1384 4-Input Data Logging Thermometer) immersed in the sample solution in close proximity to the irradiation spot. For comparison, the temperature of pure water, AuNP-pH2, and pure MWCNT (50 ± 3 μg ml^{-1}) were also measured using the same setup.

2.5. In vitro cytotoxicity test

The cytotoxicity of as-synthesized AuNP/MWCNT-pH2 nanocomposite was evaluated using the Alamar BlueTM cell viability reagent (ThermoFisher Scientific Inc. Gaithersburg, MD, USA) following the manufacturer's instruction. HeLa cells (ATCC® CCL-2TM, Manassas, VA, USA) of immortalized human cervical cells were cultured in minimum essential medium (MEM supplied by ThermoFisher Scientific Inc.) consisting of L-glutamine (3.9 mM), sodium pyruvate (1.0 mM), sodium bicarbonate (2.2 g l^{-1}) and fetal bovine serum (FBS, 10%). The HeLa cells were cultured at 37 °C in a humidified atmosphere (with 5% CO_2) until their confluency reached ~80%. HeLa cells were subsequently seeded into 96-well assay plates (Costar 3904, Corning Inc. NY, USA) with initial cell densities of 3×10^3, 4×10^3, and 5×10^3 cells per well followed by a further 24 h culture. 100 μl MWCNT, AuNP-pH2, or AuNP/MWCNT-pH2 nanocomposites solution was then added into 100 μl 2X MEM supplemented with 10% FBS and 1% Primocin (ThermoFisher Scientific Inc.) to form the test media. The cultured medium in each well of the HeLa cell culture plates was replaced with above prepared 200 μl complete medium of tested materials. Cells with new cultural media were maintained in the 37 °C incubator for 24 h (plate with 5×10^3 cells per well), 48 h (plate with 4×10^3 cells per well) and 72 h (plate with 3×10^3 cells per well), respectively. 100 μl of autoclaved double-distilled water was used as control. Cultured cells were washed twice with PBS after incubation, followed by another 2 h incubation after the complete medium containing 10% Alamar Blue® solution was added into each well. Finally, the fluorescence of these wells was measured using a POLARstar® Glomax multidetection system (Promega, Southampton, UK) with excitation/emission wavelength at 544–590 nm. Cell viability was evaluated by the relative ratio of fluorescence between test materials and control media (double-distilled water). One-way ANOVA was performed followed by Dunnett's multiple comparisons test.

3. Results and discussion

The plasma treated AuNP/MWCNT sample solutions showed distinctively different colours (figure 2(a) inset). UV–vis spectra (figure 2(a)) of all samples reveal absorption peaks at 542 nm, 547 nm, and 570 nm, which can be attributed to the surface plasmonic resonance (PR) of as-formed AuNPs within the solution [20]. It can be seen that with increasing pH, the AuNP PR peak red-shifted, which is indicative of increased AuNPs size [21]. TEM images in figures 2(b)–(d) show the morphologies of different AuNP/MWCNT nanocomposites. For AuNP/MWCNT-pH2, the AuNPs are mostly spherical in shape and are well dispersed and anchored, as individual NPs, on the surfaces of MWCNT with no evidence of AuNP agglomeration prior to anchoring (figure 2(b)). AuNPs in this sample have an average size of 28.7 ± 14.1 nm. For AuNP/MWCNT-pH7, the AuNPs attached to the MWCNT show similar spherical morphology (figure 2(c)). However, their average size is significantly larger (57.1 ± 16.8 nm) and with a lower number density. This is consistent with the shift of the PR peak observed in the UV–vis spectra as compared to that of the AuNP/MWCNT-pH2 sample. When the solution pH is adjusted to pH ~12, there is also evidence of agglomeration of the AuNPs (figure 2(d)), which may have occurred prior to the AuNPs attachment to the CNTs. The size of these AuNPs/respective agglomerates varied from 5 nm to 200 nm, which correlates well to the broadened PR peak in its UV–vis spectra. Also, the density of the anchored sites is far lower in density than in the samples synthesized at lower pH.

For comparison, we also synthesized 0.1 mM AuNPs under pH of 2, 7 and 12, under the same PiNE conditions. The PR peak of the AuNP samples exhibit a similar red-shift with increasing pH (see figure S1(a) (available online at stacks.iop.org/JPhysD/53/425207/mmedia)). However, pure AuNPs tend to exhibit more irregular shapes with agglomeration (see figures S1(b)–(d)) compared to that of AuNP/MWCNT nanocomposites. This indicates that the presence of MWCNT also plays a role in AuNP formation and its associated morphology.

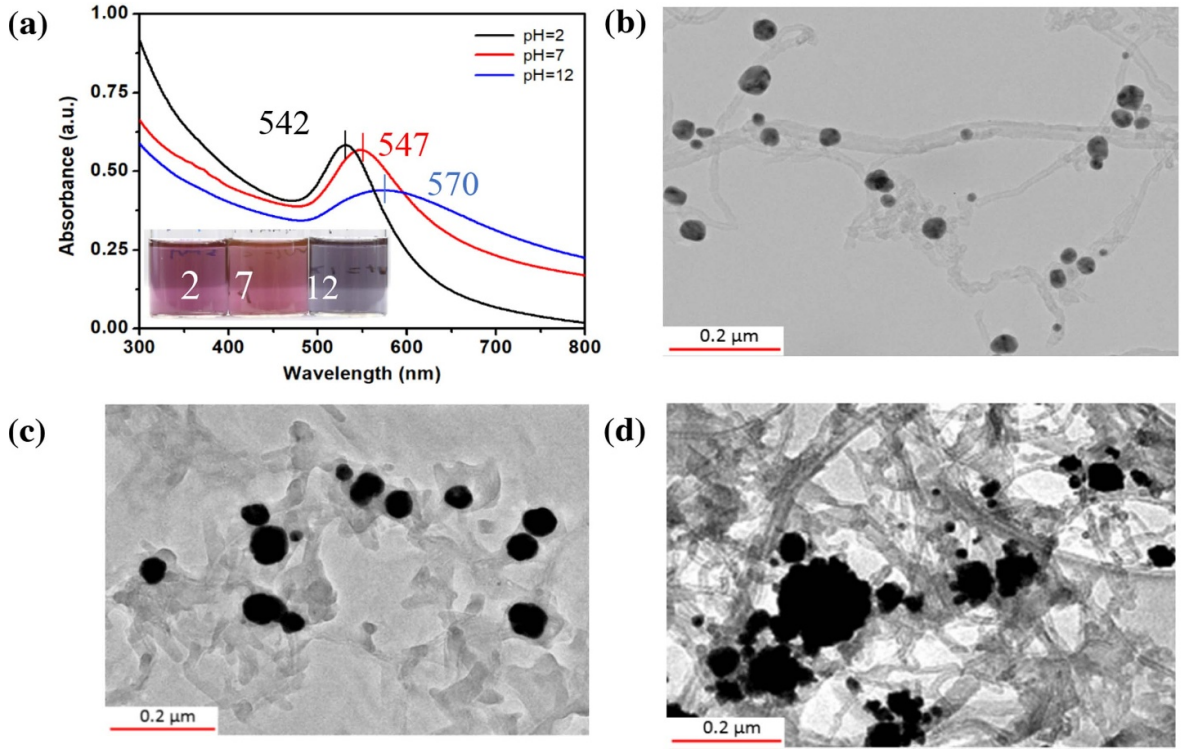

Figure 2. (a) The UV-vis spectra of AuNP/MWCNT nanocomposites synthesized from precursors with different pH; insets: corresponding optical images; (b) AuNP/MWCNT-pH2, (c) AuNP/MWCNT-pH7, and (d) AuNP/MWCNT-pH12.

Our previous work has showed that the presence of—COOH functionalities on MWCNT surface play an important role in the formation mechanism of AuNP/MWCNT nanocomposites [17]. Prior to the PiNE treatment, free $[AuCl_4]^-$ species react with deprotonated—COO^- on MWCNT surface through ion exchange interactions following equation (1) [22, 23]:

$$-COO^- + [AuCl_4]^- [-COOAuCl_3]^- + Cl^-. \quad (1)$$

This initial step reduces the concentration of Au salt in solution prior to plasma treatment and produces nucleation sites at the surface of the CNTs. Our TEM results also show that AuNPs formation occurs only at the CNT surfaces as no AuNPs were found detached from the MWCNTs. This indicates that the concentration of the remaining gold salt in solution prior to plasma treatment is not sufficient to support nucleation and growth in solution, i.e. NPs are subsequently formed only by surface growth at the $[-COOAuCl_3]^-$ sites [17]. During PiNE treatment, electrochemical and other physical/chemical phenomena are taking place at the plasma–liquid interface as well as at the solid cathode/anode. These are all interdependent and therefore it is not possible to determine which interface plays a major role; however some of the reactions and mechanisms can be described in more details. Au salt reduction at the nucleation sites and the supply of reduced gold atoms contributing to surface growth can take place through two different reaction pathways. More specifically, close to the plasma–liquid interface, both free Au ions in solution and the $[-COOHAuCl_3]$- conjugates can be directly reduced by solvated electrons following equation (2) [24, 25]:

$$Au^{3+} + 3e^- \, Au^0 \, (\text{plasma–liquid interface}). \quad (2)$$

In addition, H_2O_2 formed during the plasma–liquid interactions [11] can diffuse into bulk solution and lead to the reduction of Au ions following equation (3) [6, 26]:

$$3H_2O_2 + Au^{3+} + 3OH^- \rightarrow Au0 + 3HO2 + 3H_2O \, (\text{bulk solution}). \quad (3)$$

To clarify, the reduction induced by the short-lived hydrated electrons (equation (2)) is expected to occur close to the plasma–liquid interfaces [24, 25], while the reduction driven by H_2O_2 (equation (3)) is dominant in the bulk of the solution. Reaction 3 above is also inhibited at low pH due the lower concentration of OH^- and also at high pH where the gold salt tends to react with hydroxyl ions directly (see equation (4)). Therefore, it is expected that reduction of gold salt by hydrogen peroxide is enhanced close to neutral pH and suppressed for low/high pH values. The pH of the solution therefore influences the overall synthesis process, where two closely related outcomes have been observed. On one side, with increasing pH, the number of nucleation sites on the CNTs surfaces appear to decrease, while the NP mean size increases. The latter is merely the consequence of the former has a higher number of reduced Au atoms available per nucleation site as the pH increases, therefore leading to larger NPs. This phenomenon can be further sup-

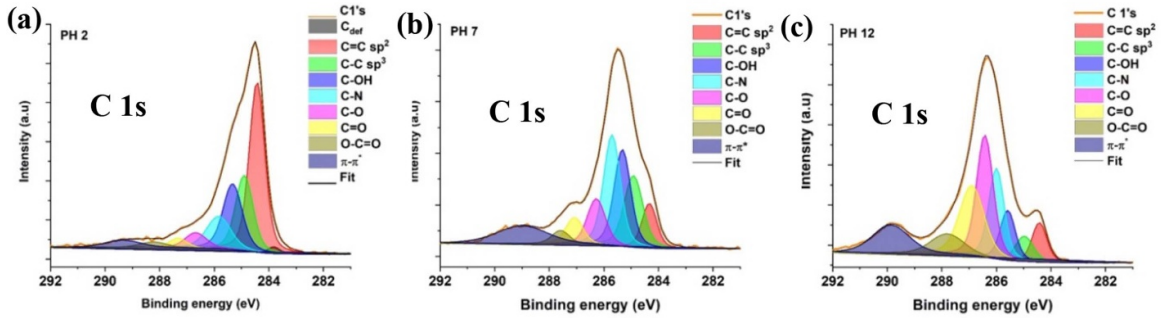

Figure 3. (a)–(c) C1s XPS spectra of AuNP/MWCNT-pH2, AuNP/MWCNT-pH7, and AuNP/MWCNT-pH12, respectively.

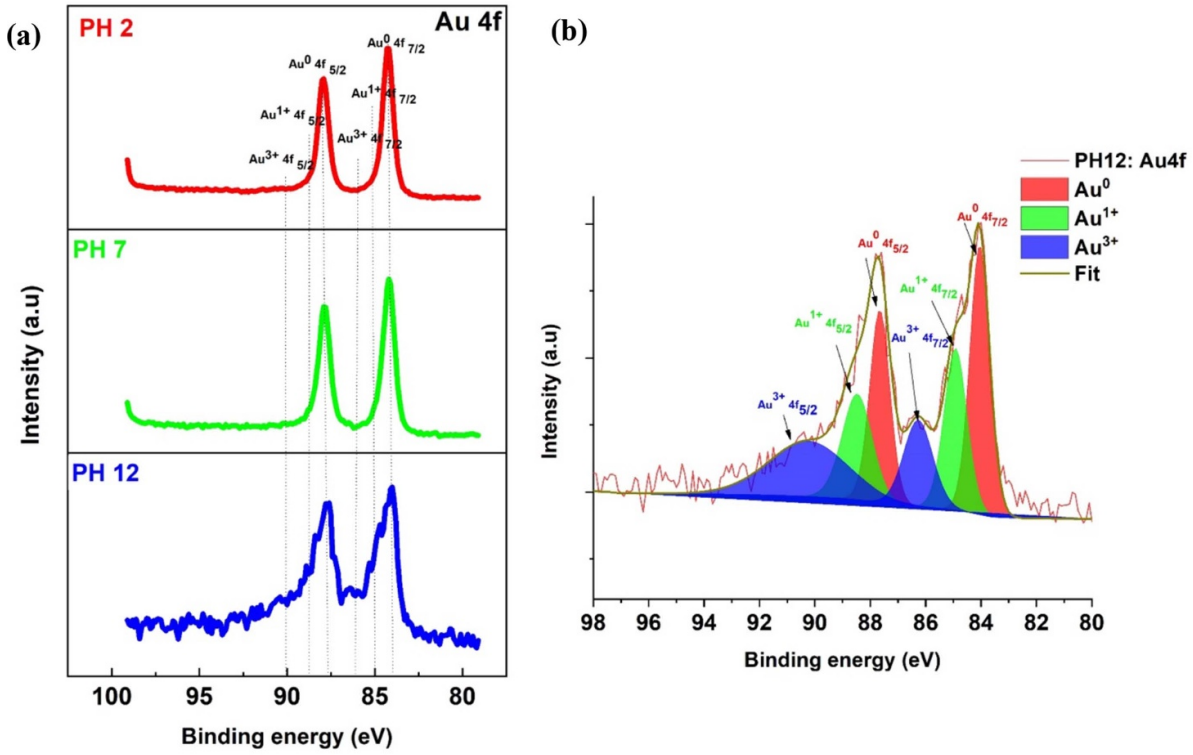

Figure 4. (a) Au 4f core XPS spectra of AuNP/MWCNT-pH2, AuNP/MWCNT-pH7, and AuNP/MWCNT-pH12, respectively; (b) de-convoluted Au 4f core peak of AuNP/MWCNT-pH12.

ported by low-magnification TEM images (see figure S2) of each AuNP/MWCNT nanocomposite synthesized under different pH.

The reduced number of nucleation sites can be explained through the interactions of OH^- with the gold salt and nucleation sites. The literature suggests that Au^{3+} complexes are present in different forms with increased solution pH [27] as shown in equation (4):

$$[AuCl_4]^- \leftrightharpoons [AuCl_3(OH)]^- \leftrightharpoons [AuCl_2(OH)_2]^- \leftrightharpoons [AuCl(OH)_3]^- \leftrightharpoons [Au(OH)_4]^- . \quad (4)$$

Note: pH increases from left to right in this equation

As the solution pH increases to pH 7 and pH 12, the $[AuCl_4]^-$ species in solution and at the nucleation sites can gradually turn into $[AuCl_{4-x}(OH)_x]^-$ (with x = 1–4). Under such pH conditions, the chance of ion exchange (equation (1)) is suppressed, hence less $[–COOHAuCl_3]^-$ sites are available for the preferential formation, nucleation and growth of AuNPs on MWCNT surfaces.

In order to gain more insight into the AuNP/CNT interaction during nanocomposites formation under different solution pH, XPS analysis was carried out to investigate C 1s and Au 4f in different samples. The C 1s of each sample were de-convoluted and results are shown in figure 3. The XPS C 1s spectra were deconvoluted into different peaks, namely, C = C (sp^2), C-C (sp^3), C-OH, C-N, C-O, C = O, O-C = O and plasmon losses π-π* and detailed fraction of each fitted component is listed in table 1 [17]. With increased solution pH, the most

Table 1. XPS analysis results of C 1s peaks for different AuNP/MWCNT nanocomposites [17].

Samples		C_{dis}	C = C	C-C	C-OH	C-N	C-O	C = O	O-C = O	Plasmon π- π^*
pH 2	BE (eV)	283.82 ± 0.05	284.43 ± 0.05	285.00 ± 0.05	285.43 ± 0.05	285.94 ± 0.05	286.78 ± 0.05	287.43 ± 0.05	288.33 ± 0.05	289.44 ± 0.05
	Fraction (%)	1%	37.70%	18.86%	18.26%	11.19%	4.72%	2.37%	2.14%	3.71%
pH 7	BE (eV)	-	284.44 ± 0.05	285.02 ± 0.05	285.42 ± 0.05	285.81 ± 0.05	286.38 ± 0.05	287.18 ± 0.05	287.76 ± 0.05	289.09 ± 0.05
	Fraction (%)		8.35%	17.05%	20.60%	23.51%	10.44%	5.85%	2.92%	11.28%
pH 12	BE (eV)	-	284.43 ± 0.05	285.00 ± 0.05	285.62 ± 0.05	286.03 ± 0.05	286.52 ± 0.05	287.03 ± 0.05	287.97 ± 0.05	289.88 ± 0.05
	Fraction (%)		6.65%	5.24	8.63%	16.05%	23.52%	19.98%	7.85%	11.87%

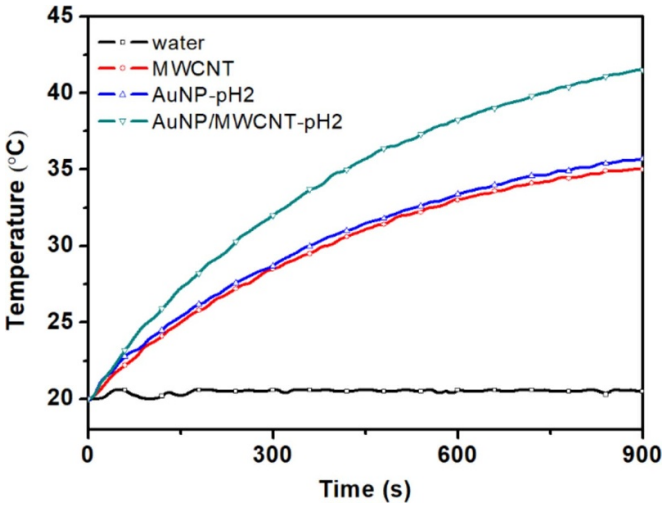

Figure 5. Photothermal response of water, MWCNT, 0.1 mM AuNP-pH2, and AuNP/MWCNT-pH2 nanocomposite under the irradiation of 455 nm laser (1 W) for 15 min.

obvious change is the relative increase of oxygen containing bonding (e.g. C-O, C = O, C-OH), which may be because less $[AuCl_4]^-$ species were available as the reaction in equation (4) progressed towards higher pH, and there is less interaction between the $[AuCl_4]^-$ species and the CNT oxygen containing surface functions.

The Au 4f core peaks of each sample are compared in figure 4(a) and the peak of AuNP/MWCNT-pH12 has been deconvoluted, see figure 4(b). It can be seen that all Au^{3+} were successfully reduced to Au^0 state when the initial solution pH was adjusted to pH 2 and pH 7. However, residual Au^{3+} is present in the AuNP/MWCNT-pH12 sample. This may be due to the higher the pH suppressed hydrogen peroxide production [28], and hence the inhibited reaction (3).

Our previous work demonstrated that the AuNP/MWCNT nanocomposites possess enhanced photothermal conversion under the NIR laser (852 nm) irradiation [17]. AuNP/MWCNT-pH2 nanocomposite demonstrated the best controlled AuNPs morphologies and the most uniform particle distribution along the CNTs. Other samples with clear sign of agglomeration may not be ideal for the proposed potential applications. In this work, PiNE synthesized AuNP/MWCNT-pH2 nanocomposites was selected as a typical sample and its response under irradiation of a 455 nm blue laser was investigated to demonstrate the potential of our nanocomposite in photothermal conversion in response to light with different wavelengths. The increase in temperature (ΔT) from room temperature serves as an indicator of the heat transfer from nanostructures to the surrounding media. As shown in figure 5, when exposed to 455 nm laser, both the MWCNT and 0.1 mM AuNP solutions exhibit a similar ΔT (~15 °C) after 15 min irradiation. In contrast, AuNP/MWCNT-pH2 shows a much higher ΔT (21.5 °C in 15 min). This result has demonstrated the capability of our as synthesized AuNP/MWCNT to convert light at a shorter wavelength into heat, which may enable its different applications such as solar thermal applications, etc [29, 30].

AuNPs and CNTs have been widely reported for applications in the field of healthcare technology, such as drug delivery [31, 32], cancer therapies [33, 34] and bio-sensing [35, 36] etc. AuNP/CNT nanocomposites are likely to offer combined functionalities/advantages of both AuNPs and CNT, and hence may enable a wider range of biomedical applications. Since the cytotoxicity is a major concern for application of nanomaterials in biological settings, we evaluated the cytotoxicity of a typical nanocomposite sample (0.1 mM AuNP/MWCNT-pH2) using established cell viability testing protocols. 0.1 mM AuNP and MWCNT solutions have been used as references, see figure 6. Results confirm that all samples tested presented no significant cytotoxicity against HeLa cells after incubation for 24 h (figure 6(a)), 48 h (figure 6(b)), and 72 h (figure 6(c)). In addition, the AuNP/MWCNT demonstrates better biocompatibility comparing to pure AuNP and MWCNT, respectively, suggesting potential future applications in the biomedical field.

In conclusion, we have investigated the effects of precursor pH on the formation AuNP/MWCNT nanocomposites synthesized by PiNE and the role of solution chemistry on the nanocomposites formation mechanisms has been elucidated. Our AuNP/MWCNT has demonstrated photothermal response under 455 nm laser irradiation and has shown minimal cytotoxicity when deployed against Hela cells. This work has offered more insights into NP formation under multi-phase (gas, plasma, CNT, AuNP, water) interaction under different precursor pH conditions. The work has also pointed to the possibility of the as synthesized AuNP/CNT nanocomposites for a wide range of applications in biomedical, solar thermal applications as well as stimulation of thermoresponsive material.

Acknowledgments

The authors would like to acknowledge the Engineering and Physical Sciences Research Council (EPSRC) for funding support (EP/P00394X/1, EP/M015211/1 and EP/R008841/1). This research has been also supported from the European Union's Horizon 2020 research and innovation programme under the Marie Skłodowska-Curie grant agreement No. 722717 (OCUTHER). Dr. Daye Sun (201606170059) thanks the China Scholarship Council (CSC) for the financial support.

ORCID iDs

Daye Sun https://orcid.org/0000-0002-8422-8381
Brian G Falzon https://orcid.org/0000-0002-3613-2924
Gianluca Sarri https://orcid.org/0000-0003-1800-343X
Davide Mariotti https://orcid.org/0000-0003-1504-4383
Paul Maguire https://orcid.org/0000-0002-2725-4647
Dan Sun https://orcid.org/0000-0002-5100-2749

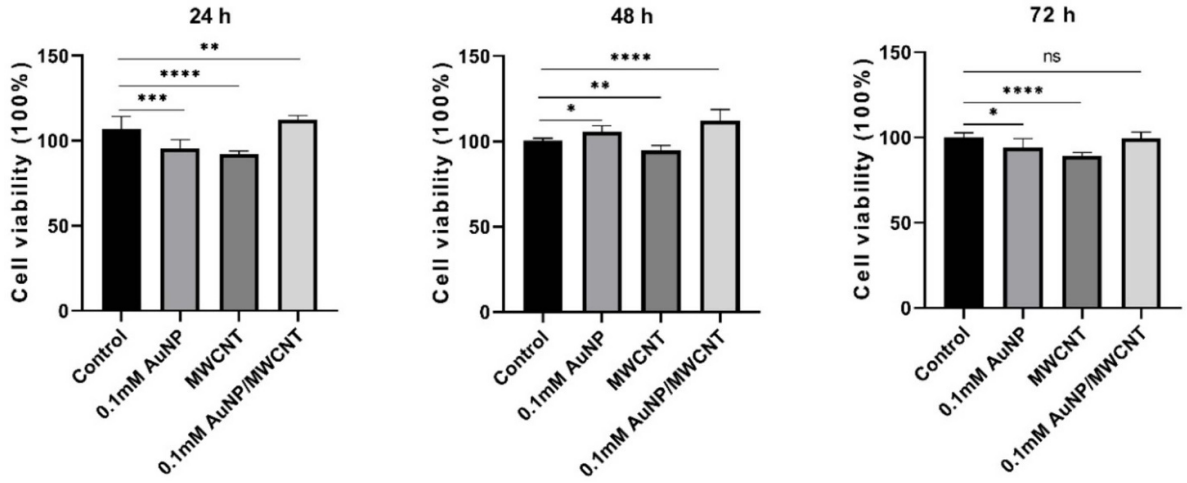

Figure 6. *In vitro* cell viability of HeLa cells after incubation with different solutions (MWCNT, 0.1 mM AuNP, and 0.1 mM AuNP/MWCNT) for 24, 48, and 72 h, respectively. One-way ANOVA followed by Dunnett's multiple comparisons test. **** $p < 0.0001$.

References

[1] Mariotti D, Patel J, Svrcek V and Maguire P 2012 Plasma-liquid interactions at atmospheric pressure for nanomaterials synthesis and surface engineering *Plasma Process. Polym.* **9** 1074–85

[2] Mariotti D and Sankaran R M 2010 Microplasmas for nanomaterials synthesis *J. Phys. D: Appl. Phys.* **43** 323001

[3] Mariotti D and Sankaran R M 2011 Perspectives on atmospheric-pressure plasmas for nanofabrication *J. Phys. D: Appl. Phys.* **44** 174023

[4] Carolan D, Rocks C, Padmanaban D B, Maguire P, Svrcek V and Mariotti D 2017 Environmentally friendly nitrogen-doped carbon quantum dots for next generation solar cells *Sustain. Energy Fuels* **1** 1611–9

[5] Askari S, Levchenko I, Ostrikov K, Maguire P and Mariotti D 2014 Crystalline Si nanoparticles below crystallization threshold: effects of collisional heating in non-thermal atmospheric-pressure microplasmas *Appl. Phys. Lett.* **104** 163103

[6] Patel J, Nmcová L, Maguire P, Graham W G and Mariotti D 2013 Synthesis of surfactant-free electrostatically stabilized gold nanoparticles by plasma-induced liquid chemistry *Nanotechnology* **24** 245604

[7] Huang X Z, Zhong X X, Lu Y, Li Y S, Rider A E, Furman S A and Ostrikov K 2013 Plasmonic Ag nanoparticles via environment-benign atmospheric microplasma electrochemistry *Nanotechnology* **24** 095604

[8] Wang R, Zuo S, Zhu W, Zhang J and Fang J 2014 Rapid synthesis of aqueous-phase magnetite nanoparticles by atmospheric pressure non-thermal microplasma and their application in magnetic resonance imaging *Plasma Process. Polym.* **11** 448–54

[9] Velusamy T, Macias-Montero A L M, Carolan D, Gherardi M, Maguire P, Svrcek V and Mariotti D 2017 Ultra-small CuO nanoparticles with tailored energy-band diagram synthesized by a hybrid plasma-liquid process *Plasma Process. Polym.* **14** e1600224

[10] Ni C *et al* 2018 Microplasma-assisted electrochemical synthesis of Co3O4 nanoparticles in absolute ethanol for energy applications *Green Chem.* **20** 2101–9

[11] Wang R, Zuo S, Wu D, Zhang J, Zhu W, Becker K H and Fang J 2014 Microplasma-assisted synthesis of colloidal gold nanoparticles and their use in the detection of cardiac Troponin I (cTn-I) *Plasma Process. Polym.* **12** 380–91

[12] Richmonds C and Sankaran R M 2008 Plasma-liquid electrochemistry: rapid synthesis of colloidal metal nanoparticles by microplasma reduction of aqueous cations *Appl. Phys. Lett.* **93** 131501

[13] Huang X, Li Y and Zhong X 2014 Effect of experimental conditions on size control of Au nanoparticles synthesized by atmospheric microplasma electrochemistry *Nanoscale Res. Lett.* **9** 572

[14] Nolan H *et al* 2018 Metal nanoparticle-hydrogel nanocomposites for biomedical applications – an atmospheric pressure plasma synthesis approach *Plasma Process. Polym.* **15** 1800112

[15] Zhang R C, Sun D, Zhang R, Lin W F, Macias-Montero M, Patel J, Askari S, McDonald C, Mariotti D and Maguire P 2017 Gold nanoparticle-polymer nanocomposites synthesized by room temperature atmospheric pressure plasma and their potential for fuel cell electrocatalytic application *Sci. Rep.* **7** 46682

[16] Sun D, Tang M, Zhang L, Falzon B G, Padmanaban D B, Mariotti D, Maguire P, Xu H, Chen M and Sun D 2019 Microplasma assisted synthesis of gold nanoparticle/graphene oxide nanocomposites and their potential application in SERS sensing *Nanotechnology* **30** 455603

[17] Sun D, McLaughlan J R, Zhang L, Falzon B G, Mariotti D, Maguire P D and Sun D 2019 Atmospheric pressure plasma synthesized gold nanoparticle/carbon nanotube hybrids for photo-thermal conversion *Langmuir* **13** 4577–88

[18] Baba K, Kaneko T, Hatakeyama R, Motomiya K and Tohji K 2010 Synthesis of monodispersed nanoparticles functionalized carbon nanotubes in plasma-ionic liquid fields *Chem. Commun.* **46** 255–7

[19] Chen Q and Shirai H, 2012 Diagnostics of atmospheric pressure microplasma with a liquid electrode *Eur. Phys. J.* D **66** 161

[20] Bastús N G, Comenge J and Puntes V 2011 Kinetically controlled seeded growth synthesis of citrate-stabilized gold nanoparticles of up to 200 nm: size focusing versus ostwald ripening *Langmuir* **27** 11098–105

[21] Haiss W, Thanh N T K, Aveyard J and Fernig D G 2007 Determination of size and concentration of gold nanoparticles from UV-Vis spectra *Anal. Chem.* **79** 4215–21

[22] Hale D K 1957 Ion exchange technology *Nature* **179** 723

[23] Zhang R, Wang Q, Zhang L, Yang S, Yang Z and Ding B 2008 The growth of uncoated gold nanoparticles on multiwalled

carbon nanotubes colloids surfaces *Physicochem. Eng. Asp.* **312** 136–41
[24] Maguire P, Rutherford D, Macias-Montero M, Mahony C, Kelsey C, Tweedie M, Pérez-Martin F, McQuaid H, Diver D and Mariotti D 2017 Continuous in-flight synthesis for on-demand delivery of ligand-free colloidal gold nanoparticles *Nano Lett.* **17** 1336–43
[25] Rumbach P, Bartels D M, Sankaran R M and Go D B 2015 The solvation of electrons by an atmospheric-pressure plasma *Nat. Commun.* **6** 7248
[26] Chen Q, Kaneko T and Hatakeyama R 2012 Reductants in gold nanoparticle synthesis using gas–liquid interfacial discharge plasmas *Appl. Phys. Express* **5** 086201
[27] Kettemann F, Birnbaum A, Witte S, Wuithschick M, Pinna N, Kraehnert R, Rademann K and Polte J 2016 Missing piece of the mechanism of the Turkevich method: the critical role of citrate protonation *Chem. Mater.* **28** 4072–81
[28] Thagard S M, Takashima K and Mizuno A 2009 Chemistry of the positive and negative electrical discharges formed in liquid water and above a gas-liquid surface *Plasma Chem. Plasma Process.* **29** 455
[29] Zedan A F, Moussa S, Terner J, Atkinson G and El-Shall M S 2013 Ultrasmall gold nanoparticles anchored to graphene and enhanced photothermal effects by laser irradiation of gold nanostructures in graphene oxide solutions *ACS Nano* **7** 627–36
[30] McGlynn R, Chakrabarti S, Alessia B, Moghaieb H S, Maguire S H and Mariotti D, 2020 Plasma-induced non-equilibrium electrochemistry synthesis of nanoparticles for solar thermal energy harvesting *Solar Energy* **203** 37–45
[31] Bianco A, Kostarelos K and Prato M 2005 Applications of carbon nanotubes in drug delivery *Curr. Opin. Chem. Biol.* **9** 674–9
[32] Tournebize J, Boudier A, Sapin-Minet A, Maincent P, Leroy P and Schneider R 2012 Role of gold nanoparticles capping density on stability and surface reactivity to design drug delivery platforms *ACS Appl. Mater. Interfaces* **4** 5790–9
[33] Ji S, Liu C, Zhang B, Yang F, Xu J, Long J, Jin C, Fu D, Ni Q and Yu X 2010 Carbon nanotubes in cancer diagnosis and therapy *Biochim. Biophys. Acta Rev. Cancer* **1806** 29–35
[34] Fazal S, Jayasree A, Sasidharan S, Koyakutty M, Nair S V and Menon D 2014 Green synthesis of anisotropic gold nanoparticles for photothermal therapy of cancer *ACS Appl. Mater. Interfaces* **6** 8080–9
[35] Kim S N, Rusling J F and Papadimitrakopoulos F 2007 Carbon nanotubes for electronic and electrochemical detection of biomolecules *Adv. Mater.* **19** 3214–28
[36] Popovtzer R *et al* 2008 Targeted gold nanoparticles enable molecular CT imaging of cancer *Nano Lett.* **8** 4593–6